Proceedings of 2008 ASME Summer Heat Transfer Conference
HT2008
August 10-14, 2008, Jacksonville, Florida, USA

HT2008-56418

THERMAL WAVE BASED MEASUREMENT OF LIQUID THERMAL CONDUCTIVITIES

Zhefu Wang*/Mechanical, Industrial, and Manufacturing Engineering
Oregon State University
Corvallis, OR, USA, 97330
Email: wangzh@engr.orst.edu

Richard B. Peterson/ Mechanical, Industrial, and Manufacturing Engineering
Oregon State University
Corvallis, OR, USA, 97330
Email: richard.peterson@oregonstate.edu

ABSTRACT

This work develops an experimental technique capable of determining thermal conductivity of liquids with application to nanofluids. A periodic current passing through a thin stainless steel strip generates a periodic Joule heating source and an infrared detector measures the temperature response at the front surface of the stainless steel strip. An open chamber is machined out of a delrin plate with the stainless steel strip acting as the sealing cover. This resulting closed chamber contains the test liquid. The phase and magnitude of the temperature response were measured using a lock-in amplifier at various frequencies from 22 to 502 Hz. A one-dimensional, two-layered transient heat conduction model was developed to predict the temperature response on the front surface of the stainless steel strip. This temperature response, including phase and magnitude, is a function of the thermal properties of the liquid. The phase information shows high sensitivity to thermal properties of the liquid layer and is employed to match experimental data to find thermal conductivities. The measured thermal conductivities of water and ethylene glycol agree well with data from the literature and support the validity of this measurement technique. An aqueous fluid consisting of gold nanoparticles was tested. Anomalous thermal conductivity enhancement was observed. Our measurement results also show a divergence of thermal transport behavior between nanofluids and pure liquids. This suggests the need to carefully examine the role of measurement techniques in the study of nanofluid heat transfer phenomena.

INTRODUCTION

Nanofluids are suspension flows with nanometer-sized (1 ~ 100 nm) particles or fibers dispersed in a base fluid. This new type of composite fluid was reported to show an anomalous enhancement of the effective thermal conductivity compared to the base fluid and claimed to be the working fluid for the next generation heat transfer applications [1, 2]. Furthermore, due to the extremely small particle size, the recently developed nanofluids seem to be able to overcome the drawbacks of the conventional suspension flows, such as clogging problems, suspension stability, surface erosion, and compatibility with the pumping systems [3]. Heat transfer enhancement of particle flows could have multiple impacts on important engineering applications, for example, electronics cooling, miniaturized energy and chemical systems, and process intensification. Therefore, thermophysical property determination of nanofluids has attracted many research studies in recent years due to the potential application of enhancing heat transfer.

Several techniques have been employed to measure thermal conductivity of nanofluids, including the transient hot-wire method [3-7], the temperature oscillation technique [8], and the optical beam deflection method [9]. However, these past experimental studies of nanofluids reveal several issues. First, measurements from different groups [3, 5] and under different techniques [8, 9] generate inconsistent results. While most of the work reported anomalous enhancement [6-8, 10-12], some presented no unpredicted thermal conductivity increase [5, 9]. Second, although the elements of heat transfer enhancement mechanisms in nanofluids were studied extensively, such as Brownian motions [13–16], interfacial layers [17, 18], aggregations [19, 20], thermophoresis [21], etc., the role of the measurement techniques on the experimental study was not examined in detail. Recently, it has been suggested that applying a measurement technique conventionally used for pure liquids to a composite liquid such as a nanofluid may lead to misinterpretation of experimental data [22]. It is desirable to

have independent experimental techniques that can provide new information about the thermal transport process in nanofluids and, therefore, help explain discrepancies among various measurement results.

The classical theory of particle/fluid systems originally proposed by Maxwell [23] successfully describes the thermal transport process of composite systems with micrometer or larger particle sizes. The composite system is treated as a homogeneous and isotropic material domain while zero thermal resistance is assumed at the solid/liquid interfaces. No relative motion between liquid and particles is another important assumption. Then, the so-called effective thermal conductivity is introduced into Fourier's law. Although this type of development fails to explain a nanofluid's abnormal capability for transferring heat, the concept of this effective thermal conductivity continues to be used in the experimental study of nanofluids. However, Vadasz [22] argued that effective thermal conductivity may not exist in a transient process which is typical for current measurement techniques, such as the transient hot-wire method. By introducing a heat transfer coefficient at the solid/liquid interface, he suggested that the transient hot-wire method may tend to overestimate the measured thermal conductivity of a composite fluid. However, no experimental data is available to provide the value of the heat transfer coefficient at the solid-liquid interface to verify his theory up to now. Therefore, if the effective thermal conductivity were still employed as a measure of thermal transport in nanofluids under the framework of Fourier's law, a single constant value of effective thermal conductivity in some narrow temperature range may not be adequate.

In light of the above discussion, this work develops a thermal wave based technique to determine thermal conductivities of nanofluids. A 12.5 μm thick stainless steel strip was periodically heated with a positive going square wave of electrical current. This stainless steel strip acted as the front surface of a test cell containing the nanofluid. A mercury cadmium telluride (HgCdTe) infrared detector sensed the temperature fluctuation on the front surface of the stainless steel strip. Both the amplitude and phase signals of the temperature response (with respect to the heating signal) on the front surface were used to determine the thermal conductivity of the fluid in the test cell. Water and ethylene glycol were used to verify the validity of this measurement technique and the measured thermal conductivities agree well with literature data. A nanofluid of gold particles in an aqueous solution with a concentration of 0.058 g/L and average particle size of 4.5 nm was tested. Measurement results show a divergence of thermal transport behavior of the nanofluid from that of pure liquids. Results also suggest a need to carefully examine the role of experimental measurement techniques in the experimental study of nanofluids, especially for the determination of quantities such as effective thermal conductivity.

NOMENCLATURE

c_p specific heat, J/kg·K
k thermal conductivity, W/m·K
g volume heating source, W/m^3
g_0 constant of volume heating source, W/m^3
n number defined in equation 8
G_0 parameter defined in equation 4
L thickness of the layer, m
T temperature, °C
t time, s
u uncertainty, %
x coordinate, m

Greek

α thermal diffusivity, m^2/s
ρ density, kg/m^3
ψ phase, degree
ω frequency, radian
ξ parameter defined in equation 5 and 6

Subscript

1 layer one
2 layer two
amp preamplifier
k thermal conductivity
l liquid
m measured
mag magnitude
ps power switch
s solid
v degree of freedom

PRINCIPLE OF MEASUREMENTS

The phase detection measurement method employed here was modified from the phase-sensitive measurement technique for determining thermal properties of a dielectric thin film [24]. Fig. 1 shows the principle of thermal conductivity measurements of fluids.

This is a one-dimensional, two-layered transient heat conduction model with a periodic volume heating source in the first layer. A stainless steel strip comprises this first layer in experiments and is 12.5 μm thick. The substrate layer is the test liquid. During the course of the study, the liquid was water, ethylene glycol, or the nanofluid.

Important assumptions of this model include:

1. One-dimensional only. Two-dimensional effect was neglected.
2. No convection occurs. Pure conduction only.
3. The liquid substrate is modeled as semi-infinite material domain.
4. The front surface of the stainless steel strip is assumed to be thermally insulated.

5. No thermal resistance exists between the stainless steel layer and the liquid substrate.
6. Constant thermal properties.

The governing differential equation for the first layer is:

$$\frac{\partial^2 T_1}{\partial x^2} + \frac{g_0 \sin(\omega t)}{k} = \frac{1}{\alpha_1}\frac{\partial T_1}{\partial t} \tag{1}$$

And the governing equation for the second layer is:

$$\frac{\partial^2 T_2}{\partial x^2} = \frac{1}{\alpha_2}\frac{\partial T_2}{\partial t} \tag{2}$$

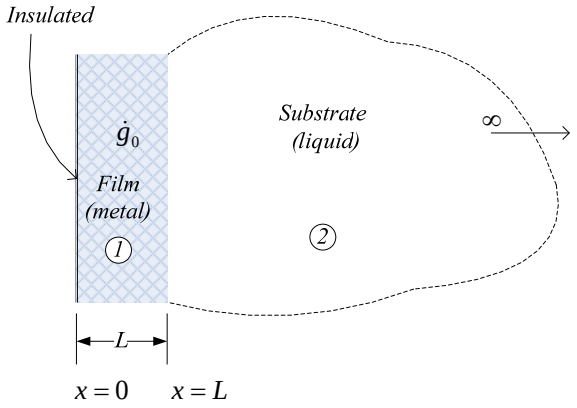

Fig. 1: Schematic diagram of the modeling domain.

Since there exists no thermal resistance between the two domains, the analytical solution becomes piecewise continuous across the interface. Both governing expressions shown in Eqs. (1) and (2) are linear and the boundary conditions are homogeneous except the heating source term. Therefore, using the method of complex combination [25], the analytical solution of the above partial differential equations can be obtained for a periodic forcing term. The complex form of the temperature expression at the front surface of layer 1 can be written as:

$$T_1(x=0,t) = e^{i\omega t} G_0 \left(1 - \frac{2}{\left(e^{-\xi_1 L} + e^{\xi_1 L}\right) + \frac{k_1 \xi_1}{k_2 \xi_2}\left(e^{\xi_1 L} - e^{-\xi_1 L}\right)} \right) \tag{3}$$

where:

$$G_0 = \frac{\alpha_1 g_0}{i\omega k_1} \tag{4}$$

$$\xi_1 = \sqrt{i\frac{\omega}{\alpha_1}} \tag{5}$$

$$\xi_2 = \sqrt{i\frac{\omega}{\alpha_2}} \tag{6}$$

In the form of a real expression, the temperature signal on the front surface of the stainless steel strip can be written as:

$$T_1(x=0,t) = T_{mag} \sin(\omega t + \psi) \tag{7}$$

where T_{mag} is the magnitude of this temperature oscillation, ω is the frequency of the heating source, and ψ is the phase shift between the heating source and the above temperature signal. A curve of the magnitude and phase shift under various frequencies can be obtained from the model developed above, which will be shown in the Results and Discussions section.

By slightly varying thermal conductivity of the substrate in the model, the sensitivities of both magnitude and phase of the temperature signal to thermal conductivity can be found. The modeling results show that the phase of the temperature signal is very sensitive to the change of thermal conductivity of the substrate liquid. For example, a 20% thermal conductivity enhancement corresponds to 0.8 to 1.2 degrees of phase shift depending on the operating frequency. However, the sensitivity of the magnitude is low and may not be practical to use the magnitude signal to detect thermal conductivity changes. Therefore, in the discussion below only the phase information will be employed to determine thermal conductivity enhancement.

The linearity of our model needs to be examined carefully before the experimental apparatus design. It is important because the heating source is a positive going square wave, not an ideal sinusoidal wave which oscillates around zero. Our model deals with the perfect sinusoidal function only. This implies that the heating source term needs to be decomposed into DC and AC components. Further, the AC component in the form of a square wave can be written as a series summation of harmonic sinusoidal functions according to Fourier's expansion,

$$g(t) = \frac{g_0}{2} + \sum_{n=1}^{\infty} \frac{2g_0}{(2n-1)\pi} \sin\left[(2n-1)\omega t\right] \tag{8}$$

Due to the linear nature of our heat conduction system, the solution also can be decomposed into AC and DC parts corresponding to the AC and DC heating source components. The DC part is the steady-state solution of the heat conduction problem with a constant heating source. It can be used to estimate the maximum temperature difference between the heating strip and the surrounding fluid and has no effect on the AC part of the solution. Each harmonic sinusoidal function in the AC part of the heating source term leads to a solution at the same frequency as shown in Eq. (7). The sum of these solutions at different frequencies comprises the AC part of the final solution. Because the solution at different frequencies can be decoupled from one another, we will focus on the solution only at the fundamental frequency and explore the relationship

between the temperature signal and thermal properties of the liquid.

In the process of designing the test cell and measurement apparatus, consideration of several basic assumptions is very important. First, the pure conduction assumption implies no natural convection inside and outside of the liquid chamber. The maximum temperature difference between the heating element and the surrounding fluid can be estimated from the steady-state heat conduction mentioned above. With the given geometry and this temperature difference, the Nussult number can be estimated. The Nussult number obtained is less than unity, which indicates that the effect of natural convection can be ignored and pure conduction assumption is valid. Second, in order to ensure that the semi-infinite material domain assumption applies, the thickness of the chamber needs to be much larger than the penetration depth of the thermal wave in our experiment [25]. According to our estimation of the maximum penetration depth in our experiment, we set the thickness of the liquid chamber to be 1.5 mm (for a liquid with the properties of water, this sets the lower frequency limit to 50 Hz). Third, because the stainless steel strip is adhesively attached to the delrin support structure at the edge, this edge effect may invalidate our one-dimensional model and suggests a wider strip. However, a wider stainless steel strip lowers the electric resistance and a detectable temperature signal at the front surface of the stainless steel strip may not be obtained. Compromise between the above two considerations suggests a width of approximately 6 mm. Also, during measurements we find an acceptable point for acquiring the signal by matching the measurement to the model in a random frequency of interest and then fixing this measurement location. This process is validated using two independent test liquids.

TEST CELL EXPERIMENTAL SETUP

Test cell preparation

The test cell holds the liquid being measured. The cell is constructed by machining an open chamber (10×6×1.5 mm) into the front surface of a piece of delrin plate (35×20×10 mm), as shown in Fig. 2. A stainless steel strip (30mm×8mm×12.5 μm) is adhesively bonded onto the delrin surface through use of a transfer tape. This covers the open side of the chamber. The metal strip works as both the heating element and the sealing surface of the test cell. Two small copper bars are soldered on the two ends of the strip to reduce the electric noise and the contact resistance between this heating strip and the contact pad. Two small stainless steel tubes connect the chamber to outside supply lines for liquid purging and refill. A polycarbonate plate with a window machined into its surface covers the stainless steel strip for protection. The sample mounting arrangement is the same as that in reference [24] except that the specimen is replaced by the test cell.

Fig. 3 shows the electric resistance of the stainless steel strip used in our experiment. The measured resistance was 0.418 Ω.

This low electrical resistance has two effects on our measurement systems. First, a large current of up to 2 Amp is needed to deliver a heating effect high enough to make the temperature oscillation detectable at 500 Hz. A MOSFET-based power switch combined with the power supply and the TTL trigger signal was developed to accommodate the high current, as shown in Fig. 4. Second, the low voltage across the heating strip due to the low resistance prohibits the direct sampling of the heating voltage signal as the reference signal to the lock-in amplifier. Also, the power switch introduces some phase shift into the measurement and needs to be compensated by other additional measurements.

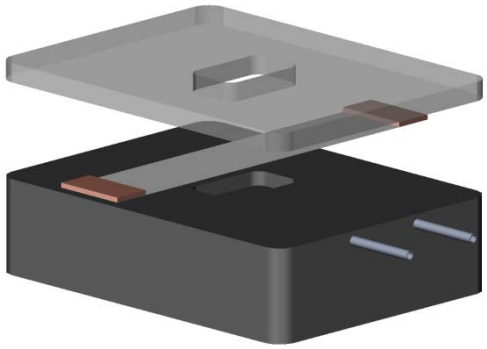

Fig. 2: Test cell design

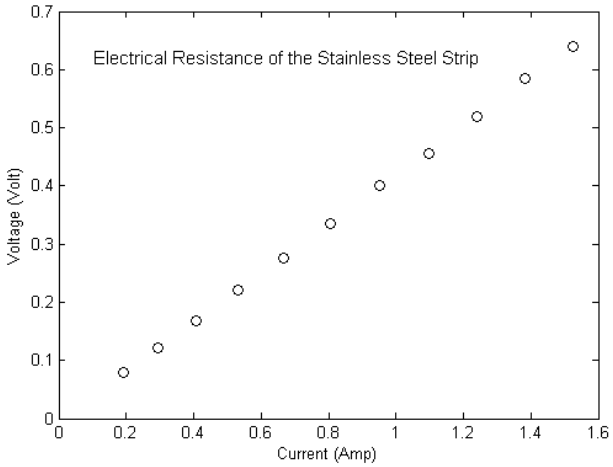

Fig. 3: Electrical resistance of the heating element.

Apparatus

The instrumentation diagram for the experiment is shown in Fig. 5, which can be divided into three sections: electrical heating, temperature sensing, and signal processing sections.

A periodic Joule heating source is generated by a periodic current passing through the stainless steel strip. This periodic current is provided by the MOSFET-based power switch, as shown in Fig. 4. The TTL square waveform from the lock-in amplifier (Stanford Research Systems model SR830) is the trigger signal to the MOSFET, while the programmable power supply (Tek model PS2520G) provides a constant voltage to the power switch. With this design, a very clear voltage square waveform up to 500 Hz can be obtained across the stainless steel strip as viewed by an oscilloscope.

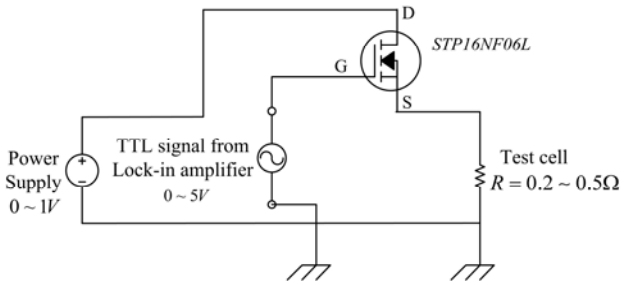

Fig. 4: Electrical diagram of the power switch.

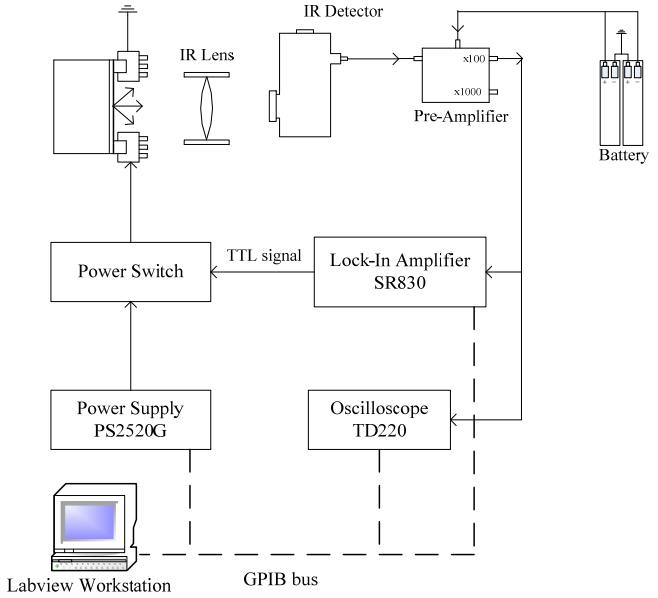

Fig. 5: System diagram of experimental apparatus.

This periodic heating source in the stainless steel strip causes the temperature oscillation on the front surface of the strip, which in turn leads to an oscillating thermal radiation signal. A zinc selenide infrared lens (Janos Technology model A1200-012) focuses this oscillating thermal radiation signal onto an infrared detector (EG&G Judson model J15D12-M204-S01M). With a bias current circuit, this mercury cadmium telluride (HgCdTe) photoconductive detector converts the absorbed radiation energy into a small voltage signal. Then, a low noise voltage preamplifier (EG&G Judson model PA-101) increases the signal strength by a factor of 100 or 1000, depending on the setting. The resulting voltage signal is supplied to the lock-in amplifier for further signal processing. Note that the preamplifier filters out the DC component so that the lock-in amplifier only receives an AC signal.

The signal processing section includes the lock-in amplifier, an oscilloscope (Tek Model TDS220), and a Labview workstation. The lock-in amplifier and the oscilloscope are connected to the Labview workstation through a GPIB bus for data logging. There are two separate paths to record and process the temperature signal. The first is to use the lock-in amplifier to record the magnitude and phase shift of the temperature signal with respect to the TTL trigger signal. The second uses the oscilloscope to record the time-varying waveforms of the temperature signal. The recorded data is then sent to the Labview workstation for further analysis.

Discussion of the signal path

One important issue that needs to be addressed is the signal transducing path. As shown in the last section, the TTL trigger signal leads to the heating source through the power switch. Then the temperature signal in form of thermal radiation energy caused by the periodic heating source is converted to a low voltage AC signal by the infrared detector. At last the pre-amplifier boosts this low voltage AC signal to a voltage level compatible to the lock-in amplifier.

However, there are two facts that prevent the direct measurement of the phase difference between the heating signal and the temperature signal using the lock-in amplifier. First is the radiation energy nature of the temperature signal. The temperature signal in form of infrared radiation needs to be converted to an electrical signal, such as a voltage signal, and this electrical signal must be compatible to the lock-in amplifier. The conversion may introduce some additional phase shift into the measurements. Second, the low signal strength and the high noise level of the heating signal precludes its being directly used as the reference input of the lock-in amplifier.

With the above considerations, the first step of our measurement procedure is to find the total phase shift of the signal path by designating the TTL trigger as reference and the pre-amplifier output as the signal input of the lock-in amplifier. After this, two compensation phase shifts need to be determined. One is the phase difference between the TTL signal and the heating signal, which is caused by the power switch and can be measured directly. Another one is the phase shift between the pre-amplifier output and the temperature signal, which is induced by the pre-amplifier and can be estimated from the electric diagram of the pre-amplifier. Therefore,

combining the above total phase shift and those two compensation phase differences together, the phase shift between the heating signal and the temperature signal will be determined. The phase shift data in the following Results section are all obtained according to the above procedure.

RESULTS AND DISCUSSIONS

The recorded temperature signal is the AC component with an operation frequency varying from 22 to 502 Hz. The maximum amplitude of the temperature oscillation is approximately 0.2°C at the lower end of the frequency range. According to the steady-state heat conduction analysis of our two-layer structure, the absolute temperature on the stainless steel surface, or the DC component, is about 28°C and 33°C with water and ethylene glycol as the test liquid, respectively.

Validation of experimental apparatus

The experimental apparatus requires a validation using liquids with well-documented thermal properties. Water and ethylene glycol were chosen for the calibration of the apparatus.

The magnitudes of the AC temperature signal for water and ethylene glycol are shown in Fig. 6. Both the modeling result and the measurement data are given. For the modeling result, the amplitudes at various frequencies are normalized by the absolute value of the signal magnitude at the highest frequency, which is at the lowest level. The same principle is applied to the experimental data. In order to display clearly, the data for ethylene glycol in this figure is shifted up by two units. For both cases of water and ethylene glycol, the normalized amplitude measurements match the model prediction very well as shown in Fig. 6.

Fig. 7 shows the phase shift data of the temperature signal. For both water and ethylene glycol, the experimental data fits the model quite well except at the lower frequency range. At low operating frequency, such as below 52 Hz, the large penetration depth causes the phase shift measurement to diverge from the model because the semi-infinite domain assumption of the liquid layer becomes problematic.

In the model developed for this study, by shifting the magnitude of the thermal conductivity a small amount from the nominal value, the sensitivity of the amplitude and phase shift to the value of thermal conductivity can be assessed. This simple analysis shows that the phase shift is much more sensitive to the variance of thermal conductivity than the amplitude. Therefore, the phase shift data will be employed below for linear regression analysis. More details will be discussed in the error analysis section.

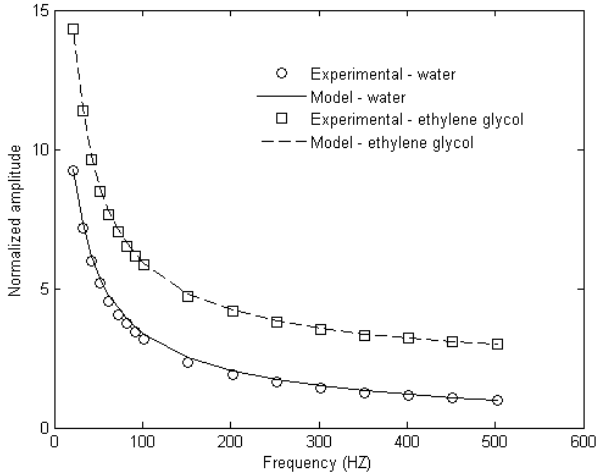

Fig. 6: Amplitude of the temperature signal

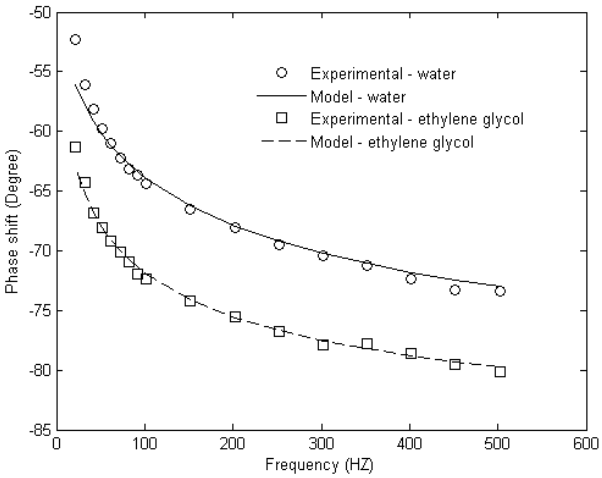

Fig. 7: Phase shift of the temperature signal

The procedure of finding the nominal value and the confidence interval of the measured thermal conductivity is as follow. First, the experimental data in the frequency range from 52 to 502 HZ were chosen by observation to avoid outliners. Second, the standard least square method is employed to find the nominal value of thermal conductivity by matching the experimental data to the model in Eq. (3). Third, the standard error of the fit is calculated with the experimental data and the model with the nominal value found in the last step. Then, the 95% confidential interval of the phase shift is obtained. Last, the 95% confidence interval of thermal conductivity was derived from that of phase shift using the least square method again.

The nominal values of thermal conductivity for water and ethylene glycol measured here are 0.614 W/m·K and 0.253

W/m·K. The 95% confidential interval is below ±3% for both the cases. The thermal conductivity of water and ethylene glycol in the literature [26] are 0.613 W/m·K and 0.252 W/m·K at 30°C.

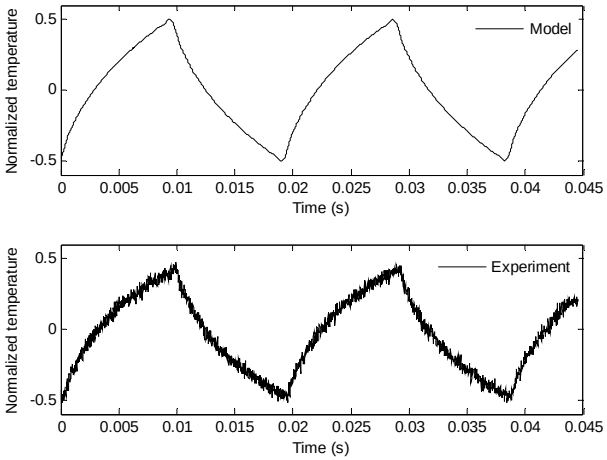

Fig. 8: The waveform of the temperature signal at 52 Hz

Another way to ensure the validity of our measurement technique is to compare the temperature signal waveform recorded from the oscilloscope to that from the analytical model. Recall that the heating signal is a square wave and can be decomposed into a series of sinusoidal functions of certain frequencies according to Fourier expansion. Because of linearity of our heat transfer system, each sinusoidal component in the heating signal will generate a temperature oscillation sinusoidal signal with the same frequency. The total temperature response will be the sum of those temperature signal sinusoidal functions.

Figure 8 shows the temperature signal waveforms at 52 Hz from the experimental measurement and the simulation of the water case. The experimental part is recorded using the oscilloscope and Labview, and the modeled curve is synthesized using the above method. The temperature scale is normalized by the maximum temperature difference for both the cases. Those two waveforms share almost the same shape.

Measurement results of nanofluid

The test nanofluid consisted of an aqueous solution with gold nanoparticles dispersed throughout the liquid. The liquid/particle mixture was generated via the citrate chemical synthesis process [27]. The concentration of gold particles was estimated to be 0.058 g/L with an average particle size of 4.5 nm with a standard deviation of 1.5 nm. Since our work concentrates on the development of measurement technique at this current stage, characterization and preparation of nanofluid will not be covered in this paper.

Before nanofluid measurement is conducted, deionized water was tested as before to calibrate the experimental apparatus and provide a reference standard for the nanofluid. After the measurement with water, the test chamber was purged with dry nitrogen and then recharged with the nanofluid through the two supply lines. All the other experimental settings were kept the same during this process in order to avoid other unaccounted for errors introduced into the measurement results.

An implicit assumption so far is that the density and heat capacity of our test liquid are fixed. By observing the temperature expression, or Eq. (3), we have determined that the thermal conductivity and heat capacity of the test liquid cannot be determined separately by our current apparatus. Because of the small volume fraction of nanoparticles, the density and heat capacity of the nanolfuid are assumed to be the same as that of the base fluid. Murshed et al. [7] conducted the measurement of effective thermal diffusivity and thermal conductivity of nanofluids simultaneously using transient hot-wire technique and suggested that the effective heat capacity of nanofluids shows little variance from the base fluid under small volume fraction. Therefore, thermal conductivity of the nanofluid is the only unknown in our model and can be predicted using the procedure of finding the nominal value described in the last section. The enhancement of the thermal conductivity of nanofluid is found to be 30.4% with the above assumptions. Once we have the enhanced thermal conductivity, the amplitude and phase shift curves can be generated, as shown in Fig. 9 and 10.

Fig. 9 shows the normalized amplitude of the temperature signal for water and the nanofluid. Again, all the data points for the nanofluid here are shifted up two units for clear display. Both measurements fit the model very well. As discussed above, this amplitude information will not be used for the estimation of the thermal conductivity enhancement because it is not sensitive to the changes of the thermal conductivity.

The phase shift data is presented in Fig. 10. Again, the experimental data for water fits the theoretical prediction quite well although some small derivation appears in the low frequency zone, i.e. below 50 Hz. For the nanofluid, good agreement is found in the high frequency zone, above approximately 150 Hz in our case. However, for the low frequency regime from 20 Hz to 150 Hz, the derivation between the experimental data and the theoretical model grows when the operating frequency decreases. Although some error was expected due to the large penetration depth effect at low frequencies, the magnitude of this discrepancy is higher than expected.

Our strategy of understanding the experimental data is to apply the concept of the effective thermal conductivity to nanofluids model first, and then identify the divergence between the theoretical model and the experimental data. For the phase shift data in Fig. 10, the phase curve fits the model of effective thermal conductivity quite well at the high

frequencies, such as above 152 Hz. Below 152 Hz, the phase shift is higher than the prediction of the model. By applying the same curve fitting method to the low frequency zone, we will have a higher effective thermal conductivity compared with that at the high frequencies. This suggests that heat transport in nanofluids tends to be more effective under the low operating frequency than that under the high operating frequency in our experiment. Our experimental results imply that a single value of the effective thermal conductivity may not be enough to describe thermal transport process in a composite system, such as nanofluids.

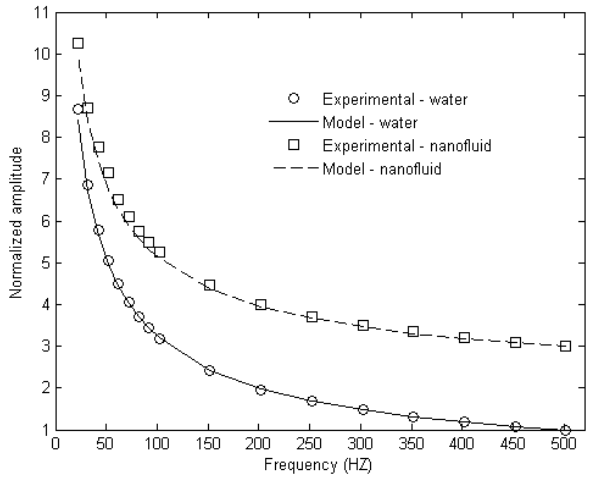

Fig. 9: The amplitude of the temperature signal

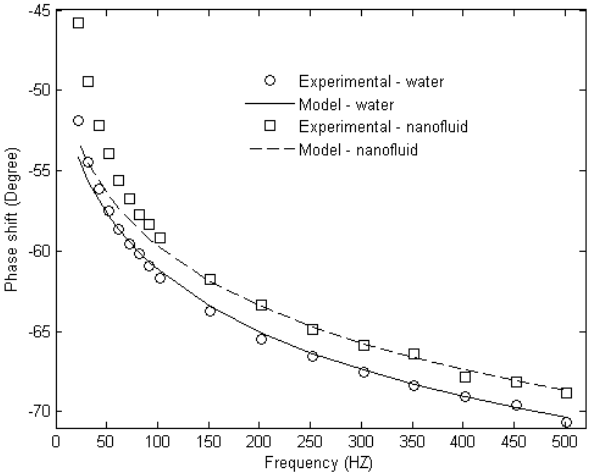

Fig. 10: The phase shift of the temperature signal

Error analysis

The measurement procedure and the parameters involved provide a guideline of our error analysis. Eq. (9) gives the related parameters in our phase shift measurement and Eq. (10) implies that thermal conductivity of the liquid is found from the measured phase shift using the curve fitting method.

Eq. (9) states that the final phase shift used to calculate the thermal conductivity of the testing liquid is a function of several parameters: the measured phase of the voltage signal from the pre-amplifier, the phase shift of the power switch, the phase shift of the pre-amplifier, thermal properties of the stainless steel, thermal properties of the liquid, the thickness of the stainless steel, and the operating frequency. To use this information, a scaling analysis of each of the above parameters will be performed to identify the main error sources first. Then, the model will be employed to find out how the error propagates from the phase shift data to the resulting value of thermal conductivity.

$$\psi = \psi\left[\psi_m, \psi_{ps}, \psi_{amp}, k_s, \rho_s, (c_p)_s, \rho_l, (c_p)_l, L, f\right] \tag{9}$$

$$k_l = k_l(\psi) \tag{10}$$

First, simple simulation shows that the thermal properties of the stainless steel are not sensitive to the phase shift of the temperature signal and can be ignored in the error analysis.

The power switch brings in an additional phase shift into the signal transferring path and needs to be quantified. With the heating signal as the input and the TTL trigger signal as reference, this phase shift can be measured. The standard deviation of this measurement result is very low and will not introduce significant uncertainty into the desired phase shift. The preamplifier introduces some phase shift into the measurement process as well. The phase shift can be calculated from the electrical diagram of the preamplifier. The calculation shows that very small errors will be brought into the final result from the preamplifier source. Thus this source can be neglected also.

The 4$^{1/2}$ digit resolution of the TTL signal generated by the lock-in amplifier implies the error from the trigger frequency f is insignificant and does not need to be considered in the error analysis. Since the thermal conductivity of the liquid is the desired property, the density and heat capacity is assumed to be constant at this development stage of the technique and no error from these liquid properties values will be considered further. Therefore, the above equations will be reduced to:

$$\psi = \psi(\psi_m, L) \tag{11}$$

$$k_l = k_l(\psi) = k_l(\psi_m, L) \tag{12}$$

The tolerance of the stainless steel strip provided by the manufacturer is 2% and will be treated as a systematic error. The error of the measured phase shift is the random uncertainty

that will propagate into the final result. The 0.01 degree phase resolution suggests that the systematic error of the lock-in amplifier can be ignored compared with that of the random error. Using the root-sum-squares (RSS) method, the uncertainty in the mean value of the thermal conductivity, u_k, is estimated from:

$$u_k = \left[\left(\frac{\partial k}{\partial L} \Delta L \right)^2 + \left(t_{v,95} \frac{\partial k}{\partial \psi} \Delta \psi \right)^2 \right]^{1/2} \quad (13)$$

By assigning different thickness values, L, to the model, the sensitivity index of the thickness, $\partial k / \partial L$, can be determined. Using the same method, we can also find the sensitivity index of the phase shift, $\partial k / \partial \psi$.

The uncertainty from the measurement of random error is fitted to be 0.0296 W/m·K, and that from the thickness tolerance of the stainless steel strip is 0.0288 W/m·K. Therefore, the total uncertainty of the thermal conductivity measurement is 0.0413 W/m·K, or about 5% of the nominal value.

CONCLUSIONS

This work describes an experimental technique that can determine the thermal conductivity of a liquid and presents the experimental results of a test case using a nannofluid with 0.058 g/L concentration gold nanoparticle. The results show a 30.4% increase of thermal conductivity compared to the base fluid with 5% uncertainty range. The experimental data of thermal conductivity also suggests a divergence from the concept of effective thermal conductivity. Future work shall be to identify promising nanofluids and use the experimental technique developed here to conduct systematic measurements.

ACKNOWLEDGMENTS

The authors gratefully acknowledge the support of the Oregon Nanoscience and Microtechnology Institute (ONAMI) and the Army Research Laboratory (ARL) for contributing to the support of this work.

REFERENCES

[1] Masuda,H., A. Ebata, K. Teramae, N. Hishinuma, 1993, “Alteration of Thermal Conductivity and Viscosity of Liquid by Dispersing Ultra-Fine Particles,” Netsu Bussei, **7**, No.4, pp. 227–233

[2] Choi, U.S., 1995, “Enhancing Thermal Conductivity of Fluids with Nanoparticles, Developments and Applications of non-Newtonian Flows,” eds. D.A. Siginer and H. P. Wang, The American Society of Mechanical Engineers, New York, FED – Vol. 231/MD – Vol.66, pp. 99-105

[3] Lee, S., S.U.S. Choi, S. Li, J.A. Eastman, 1999, “Measuring Thermal Conductivity of Fluids Containing Oxide Nanoparticles,” ASME J. Heat Transfer, **120**, pp. 280-289

[4] Patel, H.E., S.K. Das, T. Sundararajan, A.S. Nair, B. George, T. Pradeep, 2003, ‘Thermal Conductivities of Naked and Monolayer Protected Metal Nanoparticle Based Nanofluids: Manifestation of Anomalous Enhancement and Chemical Effects,” Appl. Phys. Lett., **83**, pp. 2931-2933

[5] Zhang, X., H. Gu, M. Fujii, 2006, “Experimental Study on the Effective Thermal Conductivity and Thermal Diffusivity of Nanofluids,” Int. J. Thermophys., **27**, pp. 569-580

[6] Liu, M., M. Lin, C.Y. Tsai, C.C. Wang, 2006, “Enhancement of Thermal Conductivity with Cu for Nanofluids Using Chemical Reduction Method,” Int. J. Heat Mass Transfer, **49**, pp. 3028-3033

[7] Murshed, S.M.S, K.C. Leong, C. Yang, 2006, “Determination of the Effective Thermal Diffusivity of Nanofluids by the Double Hot-wire Technique”, J. Phys. D: Applied physics, **29**, pp. 5316-5322

[8] Das, S.K., N. Putra, P. Thiesen, W. Roetzel, 2003, “Temperature Dependence of Thermal Conductivity Enhancement for Nanofluids,” ASME J. Heat Transfer, **125**, pp. 567-574

[9] Putnam, S. A., D. G. Cahill,; P. V. Braun, Z. Ge, R. G. Shimmin, 2006, “Thermal Conductivity of Nanoparticle Suspensions,” J. Appl. Phys., **99**, pp. 084308-1~6

[10] Eastman, J.A., S. Choi, S. Li, W. Yu, L.J. Thompson, 2001, “Anomalously Increased Effective Thermal Conductivities of Ethylene Glycol-based Nanofluids Containing Copper Nanoparticles,” Appl. Phys. Lett., **78**, pp. 718-720

[11] Choi, S.U.S., Z.G. Zhang, W. Yu, F.E. Lockwood, E.A. Grulke, 2001, “Anomalous Thermal Conductivity Enhancement in Nano-tube Suspension,” Appl. Phys. Lett., **79**, pp. 2252-2254

[12] Liu, M.S., M. Lin, I.T. Huang, C.C. Wang, 2006, “Enhancement of Thermal Conductivity with CuO for Nanofluids,” Chem. Eng. Technol., **29**, pp. 72-77

[13] Prasher, R., P. Bhattacharya, P.E. Phelan, 2005, “Thermal Conductivity of Nanoscale Colloidal Solutions (Nanofluids),” Phys. Rev. Lett. **94**, 025901

[14] Jang, S.P., S.U.S. Choi, 2004, “Role of Brownian Motion in the Enhanced Thermal Conductivity of Nanofluids, Appl. Phys. Lett. **84**, pp. 4316-4318

[15] Jang, S.P., S.U.S. Choi, 2007, “Effects of Various Parameters on Nanofluid Thermal Conductivity,” ASME J. Heat Transfer, **129**, pp. 617-623

[16] Prasher, R., P. Bhattacharya, P.E. Phelan, 2006, “Brownian-Motion-Based Convective-Conductive Model for the Effective Thermal Conductivity of Nanofluids,” ASME J. Heat Transfer, **128**, pp. 588-595

[17] Keblinski, P., S.R. Phillpot, S.U.S. Choi, J.A. Eastman, 2002, “Mechanisms of Heat Flow in Suspensions of

Nano-sized Particles (Nanofluids)", Int. J. Heat Mass Transfer, **45**, pp. 855-863
[18] Xie, H., M. Fujii, X. Zhang, 2003, "Effect of Interfacial Nanolayer on the Effective Thermal Conductivity of Nanoparticle-fluid Mixture," Int. J. Heat Mass Transfer, **48**, pp.2926-2932
[19] Evans, W., R. Prasher, J. Fish, P. Meakin, P. Phelan, P. Keblinski, 2008, "Effect of Aggregation and Interfacial Thermal Resistance on Thermal Conductivity of Nanocomposites and Colloidal Nanofluids," Int. J. Heat Mass Transfer, **51**, pp. 1431-1438
[20] Hong, K.S., T.K. Hong, H.S. Yang, 2006, "Thermal conductivity of Fe nanofluids depending on the cluster size of nanoparticles," Appl. Phy. Lett., **88**, pp. 031901-1–3
[21] Buongiorno, J., 2006, "Convective Transport in Nanofluids," ASME J. Heat Transfer, **128**, pp. 240-250
[22] Vadas, P., 2006, "Heat Conduction in Nanofluid Suspensions", ASME J. Heat Transfer, **128**, pp. 465- 477
[23] Maxwell, J.C., 1873, *Electricity and Magnetism*, Clarendon Press, Oxford, UK
[24] Indermuehle, S.W., R.B. Peterson, 1999, "A Phase-Sensitive Technique for the Thermal Characterization of Dielectric Thin Films," ASME J. Heat Transfer, **121**, pp. 528-536
[25] Myers, G.E., 1998, *Analytical Methods in Conduction Heat Transfer*, 2nd ed., AMCHT, Madison, WI
[26] Incropera, F.P., D.P. Dewitt, T.L. Bergman, 2006, *Fundamental of Heat and Mass Transfer,* 6th ed., Wiley, John & Sons
[27] Jackson, J.E., B.V. Borgmeyer, C.A. Wilson, P. Cheng, J.E. Bryan, 2006, "Characteristics of Nucleate Boiling with Gold Nanoparticles in Water," Proceedings of IMECE2006, ASME international mechanical engineering congress and exposition, Nov. 5-10, Chicago, IL